Development of central-upwind-WENO scheme for two-phase 1-D drift-flux model

Prasanna Welahettige[1], Christian Berg[2], Bernt Lie[1]
[1]*Department of Electrical Engineering, Information Technology and Cybernetics, University of South-Eastern Norway, Porsgrunn 3918, Norway.*
[2]*Kelda Drilling Controls, Porsgrunn, 3933, Norway.*
prasanna.welahettige@usn.no

Abstract
The two-phase drift flux model is extensively used in multiphase flow applications. In this study, we focus on possible numerical schemes for solving the drift flux model. Due to the complexity of the primitive equations and empirical parameters, it is challenging to achieve stability of the numerical scheme used for the drift flux model. The high resolution second order central scheme, the high resolution second order central-upwind scheme, and the high resolution third order and fifth order weighted essentially non-oscillatory schemes (WENO) were successfully implemented for the drift flux model. The schemes were tested with the shock tube discontinuity problem. The central-upwind-WENO scheme was developed and applied to the drift flux model. In the central-upwind-WENO scheme, the cell interface values were taken from the WENO reconstruction, and the monotone flux is calculated from the central-upwind flux. The central-upwind-WENO scheme can achieve higher order accuracy than the central-upwind scheme by using the same stencils which are used for the central-upwind scheme. The central-upwind-WENO scheme gives more accurate results than the central scheme, central-upwind scheme and the WENO scheme. Especially at the rarefaction and shock wave fronts, the central-upwind-WENO scheme gives sharper gradients compared to the other schemes. Instead of a limiter function, the central-upwind-WENO scheme uses a smoothness indicator. All the schemes used in the study are suitable for two-phase drift flux model simulation.

1. Introduction

Two-phase models are important in the oil and gas production process and in well drilling operation due to the multiphase properties of the fluid. The two-fluid model and the mixture model have been used for over two decades in the oil and gas industry. The two-fluid model treats each phase with a set of conservation equations [1]. The phase interaction appears as source terms in the conservation equations in the two-fluid model. The number of transport equations can be reduced by correlating the relative velocity between the phases, the slip velocity, with the flow variables [2] . The drift-flux model can be derived by adding together the momentum equations from both phases in the two-fluid model [3]. The drift-flux model consists of two mass conservation equations and a mixture momentum equation. The drift flux model uses a single momentum equation; therefore, it might give weak results for the phasic velocities compared to the two-fluid model. The drift flux model requires a number of empirical parameters. Those are the drawback of the drift flux model.

2. The two-phase 1-D drift flux model

Equations 1 and 2 give the mass balance for the liquid and gas phases, respectively. A single momentum equation for the liquid and gas mixture in Equation 3 gives the momentum balance for the mixture,

$$\frac{\partial(\rho_l \alpha_l)}{\partial t} + \frac{\partial(\rho_l \alpha_l v_l)}{\partial x} = 0, \quad (1)$$

$$\frac{\partial(\rho_g \alpha_g)}{\partial t} + \frac{\partial(\rho_g \alpha_g v_g)}{\partial x} = 0, \quad (2)$$

$$\frac{\partial(\rho_l \alpha_l v_l + \rho_g \alpha_g v_g)}{\partial t} + \frac{\partial(\rho_l \alpha_l v_l^2 + \rho_g \alpha_g v_g^2 + p)}{\partial x} = 0. \quad (3)$$

Here, subscripts l and g denote the liquid and gas phases, ρ is the density, α is the phase volume fraction, v is the velocity. In this study, we have not considered source terms. The drift-flux model assumes that the phases are mechanically at equilibrium, such that gas and liquid phases have same pressure, $p(x,t) = p_l(x,t) = p_g(x,t)$. The speed of sound is comparatively larger than the fluid velocity, therefore the fluids are assumed to be weakly compressible [4]. However, the phases are compressible, in other words, the densities of the phases change with time and space. The system is assumed to be isothermal; hence, the energy equation is neglected. The phases are immiscible, and there is no phase transfer between them. The pipe cross sectional area is assumed to be constant. There is set of closure laws related to the two-phase drift-flux model. There is no empty space and the total volume fraction is unity,

$$\alpha_l + \alpha_g = 1. \quad (4)$$

The closure law for the liquid density is a function of pressure,

$$\rho_l = \rho_{l,0} + \frac{1}{c_l^2}(p - p_{l,0}), \quad (5)$$

where $\rho_{l,0} = 1000$ kg/m^3 and $p_{l,0} = 1$ bar are constants related to a reference point, $c_l = 1000$ m/s is the sound velocity in the liquid phase. The closure law for the gas density as a function of pressure is

$$\rho_g = \frac{1}{c_g^2}p, \quad (6)$$

where $c_g = 316$ m/s is the sound velocity in the gas phase. The slip velocity is the relative velocity between the phases, and can be defined as a function of flow variables, $v_g - v_l = \Phi(\alpha_g, p, v_g)$ [2]. The gas velocity can be presented in term of mixture velocity, $v_m = \alpha_l v_l + \alpha_g v_g$, and gas drift velocity, v_d,

$$v_g = k v_m + v_d. \quad (7)$$

Here, k is the profile parameter (or distribution parameter); it describes the velocity and concentration profile, and is varying from 1.0 to 1.5 in a cylindrical pipe flow [3]. For simplicity, we assume $k = 1.2$; this implies that the ratio of maximum to the average flow velocity is approximately equal to 1.2. The drift velocity is 0.216 [5]. Here, we denote Equations 4, 5, 6, and 7 by the *primitive equations*.

Equation 1, 2, and 3 can be presented in compact vector form with the conservative variables,

$$\frac{\partial \mathbf{U}}{\partial t} + \frac{\partial \mathbf{F}(\mathbf{U})}{\partial x} = 0. \quad (8)$$

Here, $\mathbf{U}$ is the conservative variable vector, and $\mathbf{F}(\mathbf{U})$ is the flux vector function.

$$\mathbf{U} = \begin{pmatrix} \alpha_l\rho_l \\ \alpha_g\rho_g \\ \alpha_l\rho_l v_l + \alpha_g\rho_g v_g \end{pmatrix} = \begin{pmatrix} u_1 \\ u_2 \\ u_3 \end{pmatrix}, \quad (9)$$

$$\mathbf{F}(\mathbf{U}) = \begin{pmatrix} \alpha_l\rho_l v_l \\ \alpha_g\rho_g v_g \\ \alpha_l\rho_l v_l^2 + \alpha_g\rho_g v_g^2 + p \end{pmatrix} = \begin{pmatrix} u_1 v_l \\ u_2 v_g \\ u_1 v_l^2 + u_1 v_g^2 + p \end{pmatrix}, \quad (10)$$

while, u_1, u_2 and u_3 are conservative variables. Due to the non-linearity of the drift flux model and the closure laws, it is difficult to express explicit conservative formulas for v_l , v_g and p in the flux vector function. It is possible to express the v_l , v_g and p in terms of conservative variables. By embedding the closure laws in Equations 5 and 6 in 4, a quadratic equation can be found expressing the pressure $p(u_1, u_2)$ with conservative variables,

$$p^2 + \left(-p_0 + c_l^2\rho_{l0} - c_l^2 u_1 - c_g^2 u_2\right)p + \left(c_g^2 p_0 - c_l^2 c_g^2 \rho_{l0}\right)u_2 = 0. \quad (11)$$

Equation 11 gives two real values for the pressure; however, Equation-12 is the physically realistic root,

$$p(u_1, u_2, u_3) = 0.5\left(-\left(-p_0 + c_l^2\rho_{l0} - c_l^2 u_1 - c_g^2 u_2\right) + \sqrt{\left(-p_0 + c_l^2\rho_{l0} - c_l^2 u_1 - c_g^2 u_2\right)^2 - 4\left(c_g^2 p_0 - c_l^2 c_g^2 \rho_{l0}\right)u_2}\right). \quad (12)$$

The velocities can be derived by embedding conservative variables in Equation-7,

$$v_l(u_1, u_2, u_3) = \frac{(1-k\alpha_g)u_3 - v_d u_2}{(1-k\alpha_g)u_1 + k\alpha_l u_2}, \quad (13)$$

$$v_g(u_1, u_2, u_3) = \frac{k\alpha_l u_3 + v_d u_1}{(1-k\alpha_g)u_1 + k\alpha_l u_2}. \quad (14)$$

The fluids are assumed to be compressible. Because oil and gas reservoir pressure is comparatively large, the wells are deep, and pressure is varying along the well. Fluid densities are functions of pressure such as $\rho_l = \rho_l(u_1, u_2)$ and $\rho_g = \rho_g(u_1, u_2)$. The compact conservative form of the drift flux model, after discretization, can be presented without source terms,

$$\frac{d\mathbf{U}}{dt} = \mathbf{L}(\mathbf{U}), \quad (15)$$

Here, $\mathbf{L}(\mathbf{U})$ is the discretization of the spatial operator,

$$\mathbf{L}(\mathbf{U}) = -\frac{1}{\Delta x}\left(\mathbf{F}(\mathbf{U})_{i+\frac{1}{2}} - \mathbf{F}(\mathbf{U})_{i-\frac{1}{2}}\right). \quad (16)$$

In most applications, the challenge is to discretize the cell interface flux function, $\mathbf{F}(\mathbf{U})_{i\pm\frac{1}{2}}$, accurately. The flux function is the most important part of semi-discretization for partial differential equations. Monotonicity of the numerical flux, $\mathbf{F}(\mathbf{U})_{i+\frac{1}{2}} = \mathbf{F}\left(\mathbf{U}^+_{i+\frac{1}{2}}, \mathbf{U}^-_{i+\frac{1}{2}}\right)$, can be achieved by using monotonocity preserving schemes such as Godunov flux, Engquist-Osher flux, Lax-Friedrichs flux [6]. The positive and negative fluxes should be Lipschitz continuous functions, and should be consistent with the physical flux. Here, $\mathbf{F}\left(\mathbf{U}^+_{i+\frac{1}{2}}, \mathbf{U}^-_{i+\frac{1}{2}}\right)$ is non-decreasing in the first argument and nonincreasing in the second argument. For the lower order reconstructions, there can be a big difference between results obtained by different monotone fluxes. The order of the reconstruction polynomial higher than two helps to achieve less smearing effect at the discontinuities [7]. The problem is that most of the high order monotone schemes move to first order at a discontinuity.

3. Time integration for the semi-discrete schemes

Time integration is applied to the Equation-15. The TVD Runge-Kutta method is used to preserve the total variation diminishing (TVD) properties under the CFL condition [8]. A fourth order TVD Runge-Kutta scheme for time iterations is [9]

$$\mathbf{U}^{(1)} = \mathbf{U}^{(0)} + \frac{1}{2}\Delta t\mathbf{L}(\mathbf{U}), \quad (17)$$

$$\mathbf{U}^{(2)} = \frac{1}{2}\mathbf{U}^{(0)} + \frac{1}{2}\mathbf{U}^{(1)} - \frac{1}{4}\Delta t\mathbf{L}\left(\mathbf{U}^{(0)}\right) + \frac{1}{2}\Delta t\mathbf{L}\left(\mathbf{U}^{(1)}\right), \quad (18)$$

$$\mathbf{U}^{(3)} = \frac{1}{9}\mathbf{U}^{(0)} + \frac{2}{9}\mathbf{U}^{(1)} + \frac{2}{3}\mathbf{U}^{(2)} - \frac{1}{9}\Delta t\mathbf{L}\left(\mathbf{U}^{(0)}\right) - \frac{1}{3}\Delta t\mathbf{L}\left(\mathbf{U}^{(1)}\right) + \Delta t\mathbf{L}\left(\mathbf{U}^{(2)}\right), \quad (19)$$

$$\mathbf{U}^{(4)} = \frac{1}{3}\mathbf{U}^{(1)} + \frac{1}{3}\mathbf{U}^{(2)} + \frac{1}{3}\mathbf{U}^{(3)} + \frac{1}{6}\Delta t\mathbf{L}\left(\mathbf{U}^{(1)}\right) + \frac{1}{6}\Delta t\mathbf{L}\left(\mathbf{U}^{(3)}\right). \quad (20)$$

Here, $\mathbf{U}^{(0)}$ is related to time step n, $\mathbf{U}^{(4)}$ is related to the time step $n+1$. High order TVD Runge-Kutta methods can be found in [9]. Under the CFL restriction, the time step can be defined as,

$$\Delta t \leq c\frac{\Delta x}{\max\{\lambda_i\}\,\forall i}, \quad (21)$$

Here c is the CFL number, λ is the eigenvalues of the Jacobian of the hyperbolic system.

4. High-resolution second order central scheme for the drift flux model

The piecewise polynomials are functions of cell averages. For the third order central schemes, they couple with a piecewise quadratic approximation, such as the essentially non-oscillatory (ENO) reconstruction [10]. The integral values are approximated by the midpoint rule. The mid-point values are predicted by Taylor expansion. For more details, see [11], [12]. The cell interface values are

$$\mathbf{U}^{n,+}_{i+\frac{1}{2}} = \mathbf{U}^{n}_{i+1} - \frac{\Delta x}{2}(\mathbf{U}_x)^{n}_{i+1}, \quad (22)$$

$$\mathbf{U}^{n,-}_{i+\frac{1}{2}} = \mathbf{U}^{n}_{i} + \frac{\Delta x}{2}(\mathbf{U}_x)^{n}_{i}. \quad (23)$$

Here, the spatial derivatives, $\mathbf{U}_x$, are reconstructed from the cell averages. A scalar total variation diminishing (TVD) property is achieved from a limiter function. The family of MINMOD-like limiters are used to calculate the numerical derivative,

$$(\mathbf{U}_x)^{n}_{i} = \text{MINMOD}\left(\theta\frac{\mathbf{U}^{n}_{i}-\mathbf{U}^{n}_{i-1}}{\Delta x}, \theta\frac{\mathbf{U}^{n}_{i+1}-\mathbf{U}^{n}_{i}}{\Delta x}\right), \quad (24)$$

where, $1 \leq \theta \leq 2$ is the limiter parameter; for more details about the limiter functions, refer [13], [14]. It can be shown that for large θ values, a highly oscillatory solution is found, while for small θ values, a highly diffusive solution is found. In this study, we use the $\theta = 1$ for simplicity. The multivariable MINMOD function is defined as

$$\text{MINMOD}(z_1, z_2, \dots) = \begin{cases} \min_i\{z_i\}, & \text{if } z_i > 0, \quad \forall i, \\ \max_i\{z_i\}, & \text{if } z_i < 0, \quad \forall i, \\ 0, & \text{otherwise.} \end{cases} \quad (25)$$

The central scheme's numerical viscosity coefficient is $\frac{\Delta t}{\Delta x}a_{i+1/2}$ which is less than the numerical viscosity of the Lax-Friedrichs scheme, corresponding to the Courant-Friedrichs-Lewy (CFL) condition. There can be an accumulation of numerical dissipation, $\mathcal{O}\left(\frac{(\Delta x)^{2r}}{\Delta t}\right)$; this is one of the disadvantages of the central scheme [15]. The cell interface flux is calculated with the modified-Lax-Friedrichs scheme [12],

$$\mathbf{F}(\mathbf{U})^{n}_{i+\frac{1}{2}} = \frac{1}{2}\left(\mathbf{F}\left(\mathbf{U}^{n,-}_{i+\frac{1}{2}}\right) + \mathbf{F}\left(\mathbf{U}^{n,+}_{i+\frac{1}{2}}\right)\right) + \frac{1}{2}a^{n}_{i+\frac{1}{2}}\left(\mathbf{U}^{n,-}_{i+\frac{1}{2}} - \mathbf{U}^{n,+}_{i+\frac{1}{2}}\right). \quad (26)$$

Here, a is the one-sided local speed. In the original Lax-Friedrichs scheme, a is set as $\Delta t/\Delta x$. In this approach, a is calculated from the maximum eigenvalue of the Jacobian matrix,

$$a^{n}_{i+\frac{1}{2}} = \max\left\{\max\left\{\lambda\left(\mathbf{U}^{n,-}_{i+\frac{1}{2}}\right)\right\}, \max\left\{\lambda\left(\mathbf{U}^{n,+}_{i+\frac{1}{2}}\right)\right\}, 0\right\}. \quad (27)$$

The eigenvalues of the drift flux model are

$$\lambda = \{v_l + c_m, v_g, v_l - c_m\}. \quad (28)$$

The eigenvalues are derived with the assumption of having an incompressible liquid phase [16]. Here, c_m is the sound velocity in the mixture of gas and liquid. Based on the assumption of incompressible liquid and no slip for each phase, assuming $\alpha_g\rho_g \ll \alpha_l\rho_l$ and $0 < \alpha_g < 1$, the mixture sound velocity can be presented as [1], [17],

$$c_m = \sqrt{\frac{p}{\alpha_g\rho_l(1-k\alpha_g)}}. \quad (29)$$

Here we introduce the stencils for the central scheme in a form similar to that of ENO schemes. To calculate the cell interface function, the second order central scheme uses one stencil from one side, because the MINMOD limiter function selects a single stencil from a side.

5. Second order central-upwind scheme for the drift flux model

As an improvement of the high-resolution central scheme, the central-upwind scheme was developed by Kurganov et al. [15]. The scheme is a semi-discrete scheme, Godunov-type central scheme since it is based on integration over the Riemann fan. The upwind nature of the scheme is adapted by measuring the one-sided local speeds which present the directions of wave propagation. The one-sided propagation speeds are the largest and smallest eigenvalues of the Jacobian matrix at the cell interface. The central-upwind scheme is a Godunov-type central scheme because the evolution employs the integration over the Riemann solver, and it does not require a Riemann solver and a characteristic decomposition. Equation 22 and 23 calculate the cell interface values, $\mathbf{U}^{n,\pm}_{i+\frac{1}{2}}$, with the MINMOD limiter function. Compared with the high-resolution central scheme, the high-resolution central-upwind scheme only differs is the cell interface flux calculation. Specifically, the central-upwind scheme consists of negative and positive direction one-sided local speeds at the cell interface. These are called the discontinuities propagation speeds. The discontinuities propagation speeds in right and left sides are

$$a_{i+\frac{1}{2}}^{n,+} = \max\left\{\max\left\{\lambda\left(\mathbf{U}_{i+\frac{1}{2}}^{n,-}\right)\right\}, \max\left\{\lambda\left(\mathbf{U}_{i+\frac{1}{2}}^{n,+}\right)\right\}, 0\right\}, \quad (30)$$

$$a_{i+\frac{1}{2}}^{n,-} = \min\left\{\min\left\{\lambda\left(\mathbf{U}_{i+\frac{1}{2}}^{n,-}\right)\right\}, \min\left\{\lambda\left(\mathbf{U}_{i+\frac{1}{2}}^{n,+}\right)\right\}, 0\right\}. \quad (31)$$

The central-upwind scheme bounds the Riemann fan by $\left(a_{i+\frac{1}{2}}^{n,+} - a_{i+\frac{1}{2}}^{n,-}\right)\Delta t$ [15]. The numerical flux of the high resolution central-upwind scheme is

$$\mathbf{F}(\mathbf{U})_{i+\frac{1}{2}}^{n} = \frac{a_{i+\frac{1}{2}}^{n,+}\mathbf{F}\left(\mathbf{U}_{i+\frac{1}{2}}^{n,-}\right) - a_{i+\frac{1}{2}}^{n,-}\mathbf{F}\left(\mathbf{U}_{i+\frac{1}{2}}^{n,+}\right)}{a_{i+\frac{1}{2}}^{n,+} - a_{i+\frac{1}{2}}^{n,-}} + \frac{a_{i+\frac{1}{2}}^{n,+}a_{i+\frac{1}{2}}^{n,-}}{a_{i+\frac{1}{2}}^{n,+} - a_{i+\frac{1}{2}}^{n,-}}\left(\mathbf{U}_{i+\frac{1}{2}}^{n,+} - \mathbf{U}_{i+\frac{1}{2}}^{n,-}\right). \quad (32)$$

The numerical flux, $\mathbf{F}(\mathbf{U})_{i+\frac{1}{2}}^{n}$, is independent of Δt, therefore the numerical viscosity is independent of $\mathcal{O}\left(\frac{1}{\Delta t}\right)$ in both the central and the central-upwind schemes. This is an advantage for using these two schemes for steady state calculations. The order of the scheme is second order.

6. WENO scheme for the drift flux model

Harten et al. [10] made the fundamental step for developing the ENO scheme. The ENO scheme uses a non-linear adaptive procedure to select the smoothest stencil where it can avoid the crossing discontinuities as much as possible [7]. ENO schemes map the cell averages in the stencil to the value of cell interface where there exists constant values. As the first step of the ENO scheme, a polynomial reconstruction is used to approximate the cell averages. If the degree of the interpolation polynomial function is r, then the order of the ENO scheme becomes r. The weighted ENO (WENO) scheme can be generated from the same stencil node in the ENO scheme with higher order accuracy. Liu et al. [6] developed the WENO scheme and it is further developed by Jiang and Shu [19]. The WENO scheme uses a convex combination of all the candidate stencils instead of just one used in the ENO scheme. Therefore, the WENO scheme can achieve higher order accuracy, $2r-1$, by using the same ENO stencils.

6.1. Fifth order WENO scheme for the drift flux model

Parallel to the third order ENO scheme, the fifth order WENO scheme uses a convex combination of the all three stencils [20].

The third order ENO approach is used to calculate the cell interface variable related to each stencil. The negative direction cell interface with related to the stencils s_0, s_1, and s_2 are

$$\mathbf{U}_{i+\frac{1}{2}}^{-,0} = \frac{1}{3}\mathbf{U}_{i-2} - \frac{7}{6}\mathbf{U}_{i-1} + \frac{11}{6}\mathbf{U}_i, \quad (33)$$

$$\mathbf{U}_{i+\frac{1}{2}}^{-,1} = -\frac{1}{6}\mathbf{U}_{i-1} + \frac{5}{6}\mathbf{U}_i + \frac{1}{3}\mathbf{U}_{i+1}, \quad (34)$$

$$\mathbf{U}_{i+\frac{1}{2}}^{-,2} = \frac{1}{3}\mathbf{U}_i + \frac{5}{6}\mathbf{U}_{i+1} - \frac{1}{6}\mathbf{U}_{i+2}. \quad (35)$$

The positive direction cell interface with related to the stencils s_0, s_1, and s_2 are

$$\mathbf{U}_{i+\frac{1}{2}}^{+,0} = \frac{11}{6}\mathbf{U}_{i+1} - \frac{7}{6}\mathbf{U}_{i+2} + \frac{1}{3}\mathbf{U}_{i+3}, \quad (36)$$

$$\mathbf{U}_{i+\frac{1}{2}}^{+,1} = \frac{1}{3}\mathbf{U}_i + \frac{5}{6}\mathbf{U}_{i+1} - \frac{1}{6}\mathbf{U}_{i+2}, \quad (37)$$

$$\mathbf{U}_{i+\frac{1}{2}}^{+,2} = -\frac{1}{6}\mathbf{U}_{i-1} + \frac{5}{6}\mathbf{U}_i + \frac{1}{3}\mathbf{U}_{i+1}. \quad (38)$$

Here we have skipped the superscript n in time. The cell averages are used to calculate the cell interface value $\mathbf{U}_{i+\frac{1}{2}}^{\pm}$in each stencil. Here we only present the left side stencils approach. The convex combination of the left biased stencils of the ENO approach gives the WENO approach, at the cell interface $i+\frac{1}{2}$,

$$\mathbf{U}_{i+\frac{1}{2}}^{-} = \omega_0\mathbf{U}_{i+\frac{1}{2}}^{-,0} + \omega_1\mathbf{U}_{i+\frac{1}{2}}^{-,1} + \omega_2\mathbf{U}_{i+\frac{1}{2}}^{-,2}. \quad (39)$$

The weight functions are

$$\omega_0 = \frac{\alpha_0}{\alpha_0+\alpha_1+\alpha_2}, \quad (40)$$

$$\omega_1 = \frac{\alpha_1}{\alpha_0+\alpha_1+\alpha_2}, \quad (41)$$

$$\omega_2 = \frac{\alpha_2}{\alpha_0+\alpha_1+\alpha_2}, \quad (42)$$

Here, $\omega_0+\omega_1+\omega_2 = 1$, and

$$\alpha_0 = \frac{1/10}{(\epsilon+\beta_0)^2}, \quad (43)$$

$$\alpha_1 = \frac{6/10}{(\epsilon+\beta_1)^2}, \quad (44)$$

$$\alpha_2 = \frac{3/10}{(\epsilon+\beta_2)^2}. \quad (45)$$

$\epsilon = 10^{-6}$ is used to avoid division by zeroβ is the smoothness indicator. The smoothness indicator is defined based on undivided differences [20]. The smoothness indicator consists of a $(r-1)$-th order accurate polynomial functions,

$$\beta_0 = \frac{13}{12}(\mathbf{U}_{i-2} - 2\mathbf{U}_{i-1} + \mathbf{U}_i)^2 + \frac{1}{4}(\mathbf{U}_{i-2} - 4\mathbf{U}_{i-1} + 3\mathbf{U}_i)^2, \quad (46)$$

$$\beta_1 = \frac{13}{12}(\mathbf{U}_{i-1} - 2\mathbf{U}_i + \mathbf{U}_{i+1})^2 + \frac{1}{4}(\mathbf{U}_{i-1} - \mathbf{U}_{i+1})^2, \quad (47)$$

$$\beta_2 = \frac{13}{12}(\mathbf{U}_i - 2\mathbf{U}_{i+1} + \mathbf{U}_{i+2})^2 + \frac{1}{4}(3\mathbf{U}_i - 4\mathbf{U}_{i+1} + \mathbf{U}_{i+2})^2. \quad (48)$$

By symmetry, the $\mathbf{U}_{i+\frac{1}{2}}^{+}$ values can be calculated. Here we choose the local Lax-Friedrichs flux to calculate the monotone flux in the WENO scheme. The local Lax-Friedrichs flux is

$$\mathbf{F}(\mathbf{U})_{i+\frac{1}{2}}^{n} = \mathbf{F}\left(\frac{\mathbf{U}_{i+\frac{1}{2}}^{n,-} + \mathbf{U}_{i+\frac{1}{2}}^{n,+}}{2}\right) - \frac{1}{2}a_{i+\frac{1}{2}}^{n}\left(\mathbf{U}_{i+\frac{1}{2}}^{n,-} - \mathbf{U}_{i+\frac{1}{2}}^{n,+}\right), \quad (49)$$

where $a_{i+\frac{1}{2}}^{n}$ is

$$a_{i+\frac{1}{2}}^{n} = \max\left\{\max\left\{\lambda\left(\mathbf{U}_{i+\frac{1}{2}}^{n,-}\right)\right\}, \max\left\{\lambda\left(\mathbf{U}_{i+\frac{1}{2}}^{n,+}\right)\right\}\right\}. \quad (50)$$

6.2. Third order WENO scheme for the drift flux model

The third order WENO scheme is developed from the second-order ENO scheme. Parallel to the fifth order WENO scheme, the third order WENO scheme has two stencils in each side. Here we briefly explain the third order WENO scheme, one can compare the fifth order WENO scheme parallelly. The cell interface values for the stencil s_0 and s_1 respectively are

$$\mathbf{U}^{-,0}_{i+\frac{1}{2}} = -\frac{1}{2}\mathbf{U}_{i-1} + \frac{3}{2}\mathbf{U}_i, \quad (51)$$

$$\mathbf{U}^{-,1}_{i+\frac{1}{2}} = \frac{1}{2}\mathbf{U}_i + \frac{1}{2}\mathbf{U}_{i+1}. \quad (52)$$

The negative cell interface value is

$$\mathbf{U}^{-}_{i+\frac{1}{2}} = \omega_0\mathbf{U}^{-,0}_{i+\frac{1}{2}} + \omega_1\mathbf{U}^{-,1}_{i+\frac{1}{2}}. \quad (53)$$

The weight functions are

$$\omega_0 = \frac{\alpha_0}{\alpha_0+\alpha_1}, \quad (54)$$

$$\omega_1 = \frac{\alpha_1}{\alpha_0+\alpha_1}, \quad (55)$$

where,

$$\alpha_0 = \frac{1}{(\epsilon+\beta_0)^2}, \quad (56)$$

$$\alpha_1 = \frac{1}{(\epsilon+\beta_1)^2}, \quad (57)$$

and,

$$\beta_0 = (\mathbf{U}_{i-1} - \mathbf{U}_i)^2, \quad (58)$$

$$\beta_1 = (\mathbf{U}_i - \mathbf{U}_{i+1})^2. \quad (59)$$

The right side (positive direction) functions can be found by symmetry to the cell interface $i + \frac{1}{2}$.

7. Proposing a high resolution central-upwind-WENO scheme for the drift flux model

Here we use the above mentioned central scheme, the central-upwind scheme, and the WENO scheme for development of a central-upwind-WENO scheme. The main idea of the central-upwind-WENO scheme is to calculate the numerical flux from the central-upwind flux, and the cell interface values are calculated from the WENO reconstruction. The objective is to adapt the central-upwind nature in WENO scheme which can produce more accurate and stable results. The order of the scheme is decided by the polynomial interpolation used to calculate the cell interface flux.

7.1. Development of high resolution fifth order central-upwind-WENO scheme for the drift flux model

The cell interface flux is calculated with the central-upwind flux. Here we rewrite Equation 32 which gives the central-upwind flux,

$$\mathbf{F}(\mathbf{U})^n_{i+\frac{1}{2}} = \frac{a^{n,+}_{i+\frac{1}{2}}\mathbf{F}\left(\mathbf{U}^{n,-}_{i+\frac{1}{2}}\right) - a^{n,-}_{i+\frac{1}{2}}\mathbf{F}\left(\mathbf{U}^{n,+}_{i+\frac{1}{2}}\right)}{a^{n,+}_{i+\frac{1}{2}} - a^{n,-}_{i+\frac{1}{2}}} + \frac{a^{n,+}_{i+\frac{1}{2}}a^{n,-}_{i+\frac{1}{2}}}{a^{n,+}_{i+\frac{1}{2}} - a^{n,-}_{i+\frac{1}{2}}}\left(\mathbf{U}^{n,+}_{i+\frac{1}{2}} - \mathbf{U}^{n,-}_{i+\frac{1}{2}}\right). \quad (60)$$

The one-sided local speeds in Equation 60 can be calculated from the largest and smallest eigenvalues of the system. Here we rewrite the Equations 25 and 26 form of the central-upwind scheme:

$$a^{n,+}_{i+\frac{1}{2}} = \max\left\{\max\left\{\lambda\left(\mathbf{U}^{n,-}_{i+\frac{1}{2}}\right)\right\}, \max\left\{\lambda\left(\mathbf{U}^{n,+}_{i+\frac{1}{2}}\right)\right\}, 0\right\}, \quad (61)$$

$$a^{n,-}_{i+\frac{1}{2}} = \min\left\{\min\left\{\lambda\left(\mathbf{U}^{n,-}_{i+\frac{1}{2}}\right)\right\}, \min\left\{\lambda\left(\mathbf{U}^{n,+}_{i+\frac{1}{2}}\right)\right\}, 0\right\}. \quad (62)$$

The cell interface values $\mathbf{U}^{n,\pm}_{i+\frac{1}{2}}$ can be calculated from the fifth order WENO reconstruction. Here, we rewrite Equation 39, which gives the negative direction cell interface value,

$$\mathbf{U}^{-}_{i+\frac{1}{2}} = \omega_0\mathbf{U}^{-,0}_{i+\frac{1}{2}} + \omega_1\mathbf{U}^{-,1}_{i+\frac{1}{2}} + \omega_2\mathbf{U}^{-,2}_{i+\frac{1}{2}}. \quad (63)$$

The weight functions can be calculated from Equations 40 to 48. The fifth order central-upwind-WENO scheme is developed from the central-upwind flux and the fifth order WENO reconstruction for the cell interface values. Once we know the cell interface flux, it is possible to calculate flux gradients.

7.2. Development of high resolution third order central-upwind-WENO scheme for the drift flux model

Like the fifth order central-upwind-WENO scheme, the third order central-upwind-WENO scheme can be developed. The numerical flux function is calculated from the Equations 60 to 62. The cell interface values can be calculated from Equations 51 to 59.

8. Results

The shock tube problem is a benchmark case for testing the capability of numerical schemes in pipe flow. Evje and Flåtten [1] used the following initial conditions for a discontinuity in a pipe flow, see Figure 1. Here, subscript L is left side and subscript R is right side.

$p_L = 80450$ Pa	$p_R = 24282$ Pa
$\alpha_g = 0.55$	$\alpha_g = 0.55$
$v_L = 10.37$ m/s	$v_L = 0.561$ m/s

Figure 1. Initial condition of the shock tube problem-1 in the pipe flow

The initial gas velocity, v_g, can be calculated as, $v_g = (kv_l\alpha_l + v_d)/(1 - k\alpha_l)$. For the test case, we assume that the diameter of the pipe is 0.1 m, the length of the pipe is 100 m, the step length is Δx = 0.5 m. The initial discontinuity is at x = 50 m when t = 0 s. The friction force and gravity force terms are neglected for the numerical test, and $k = 1.07$ and $v_d = 0.216$ m/s. The test problem is purely a convection dominated flow; this initial condition generates discontinuities for all three conservative variables. The fifth order WENO scheme with fine mesh is used as the reference solution; we used 2.5

times more cells in the fluid domain compared to the other schemes. The fifth order WENO scheme gives accurate results compared with [16]. Figure 2 shows the shock tube problem result comparison between the central-upwind-WENO scheme and the central scheme. The results are shown after 1 s of simulation for pressure, gas velocity, liquid velocity, and liquid volume fraction. The central-upwind-WENO scheme gives a better solution than the central scheme, especially at the square wave in the solution. The second order central scheme is more diffusive compared to the other schemes used in this study. Figure 3 shows the shock tube result comparison between the third order central-upwind-WENO scheme vs. the second order central-upwind scheme. Compared to the central scheme, the central-upwind scheme gives more accurate results. However, the central-upwind-WENO scheme gives even higher accuracy than the central-upwind scheme. Figure 4 shows the shock tube problem result after 1s of simulation for the third order central-upwind-WENO scheme vs. the third order WENO scheme. The third order WENO scheme gives more accurate results than the central scheme and the central-upwind scheme. However, the third order central-upwind-WENO scheme gives more accurate results than the third order WENO scheme. The third order central-upwind-WENO scheme gives sharper gradient for rarefaction waves and shock wave fronts compared to the third order WENO scheme, the second order central scheme, and the second order central-upwind scheme. In other words, the third-order central-upwind-WENO gives the highest accuracy.

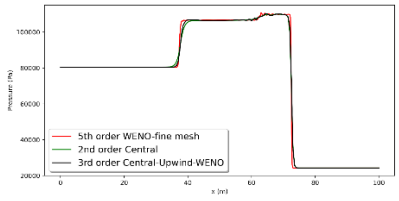

(a)

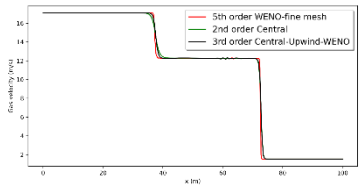

(b)

Figure 2. Shock tube problem results comparison after 1 s simulation between the third order high-resolution central-upwind-WENO scheme vs. the second order high-resolution central scheme. The fifth order WENO scheme with a fine mesh is used as the reference: (a)Pressure, (b)Gas velocity.

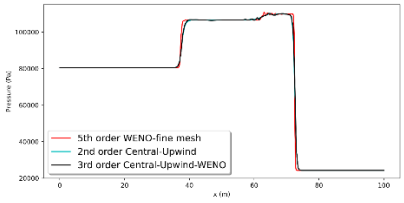

(a)

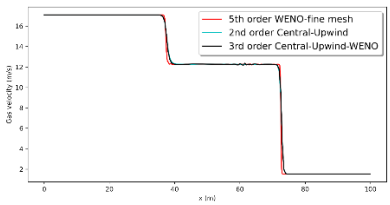

(b)

Figure 3. Shock tube problem results comparison after 1 s simulation between the third order high-resolution central-upwind-WENO scheme vs. the second order high-resolution central-upwind scheme. The fifth order WENO scheme with a fine mesh result is used as the reference: (a)Pressure, (b)Gas velocity.

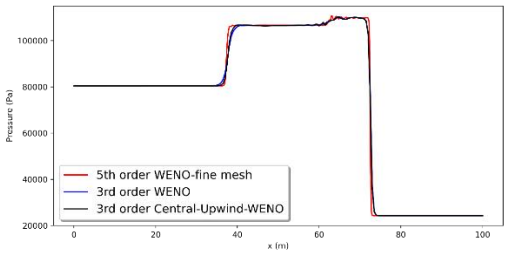

(a)

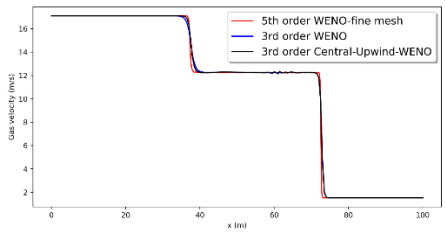

(b)

Figure 4. Shock tube problem results comparison after 1 s simulation between the third order high-resolution central-upwind-WENO scheme vs. the third order high-resolution WENO scheme. The fifth order WENO scheme with a fine mesh result is used as the reference: (a)Pressure, (b)Gas velocity.

Table 1 shows the computational speed comparison for the schemes. The simulations have conducted for the shock tube problem up to 1s, and all the schemes have used same coarse mesh which has 200 cells. The CPU times presented in the table are averages of five simulation runs for each case. The third order WENO scheme is the fastest scheme, it has higher

accuracy than the second order central scheme and second order central-upwind scheme. Compared to the third order WENO scheme, the central-upwind scheme is a slower scheme. The MINMOD limiter function has logical "if" closure structures, or equivalent mathematical formulae, which are not very efficient. The WENO scheme solves algebraic equations with weight functions. Therefore, the central and the central-upwind second order schemes are slower than the third order WENO scheme. However, all the schemes are in same speed range, this is no big differences. One can argue that fifth order WENO scheme has comparatively high speed for the coarse mesh. However, the fifth order WENO scheme gives higher oscillatory results for the coarse mesh than the third order WENO schemes, see Figure 5. The fifth order WENO scheme is very accurate and less oscillatory for finer mesh. The fifth order central-upwind-WENO scheme is more accurate than the fifth order WENO scheme. However, the fifth order WENO scheme and the fifth order central-upwind-WENO scheme produce more oscillatory results than their third order schemes.

Table 1: Computational time comparison: Computation time was calculated for 1s simulations. All the schemes were used same coarse mesh, 200 cells

Scheme	**CPU Time (s)**
Third order central-upwind-WENO	0.90
Fifth order WENO	0.95
Third order WENO	0.80
Second order central	0.88
Second order central-upwind	0.92

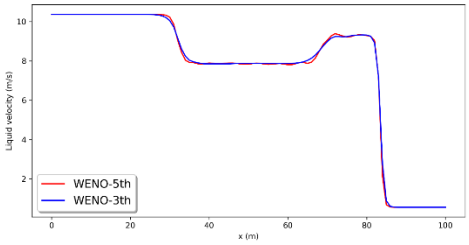

Figure 5. Coarse mesh simulation of the fifth order WENO scheme and the third order WENO scheme: The mesh has 200 cells. The results show liquid velocity for the shock tube problem

9. Concluding remarks

In this study, we considered possible numerical schemes for the two-phase drift flux model. The drift flux model is typically used in well-drilling and oil-gas production process in the petroleum industry. The high resolution second order central scheme, the high resolution second order central-upwind scheme and the third order and fifth order WENO schemes were used for numerical simulations. The stencil selection procedure and numerical discretization procedure were explained in detailed for each scheme. We developed the high resolution third order and fifth order central-upwind-WENO scheme for the drift flux model. The main idea of the central-upwind-WENO scheme is to calculate the numerical flux from the central-upwind flux, and the cell interface values are calculated from the WENO reconstruction. This method helps to achieve higher order of the scheme with minimum number of stencils. The developed central-upwind-WENO scheme produces more accurate results than the central scheme, the central-upwind scheme, and the WENO scheme. All the schemes used in the study are suitable for the drift-flux model simulation. The source term effect, especially friction and gravity, will be discussed in future publications.

Acknowledgement

We gratefully acknowledge the economic support from The Research Council of Norway and Equinor ASA through project no. 255348/E30 "Sensors and models for improved kick/loss detection in drilling (Semi-kidd)".

References

[1] S. Evje and T. Flåtten, "Hybrid flux-splitting schemes for a common two-fluid model," *Journal of Computational Physics*, vol. 192, no. 1, pp. 175–210, 2003, doi: 10.1016/j.jcp.2003.07.001.

[2] S. T. Munkejord, *Analysis of the two-fluid model and the drift-flux model for numerical calculation of two-phase flow*, no. November. 2005.

[3] H. Shi *et al.*, "Drift-flux modeling of two-phase flow in wellbores," *SPE Journal*, vol. 10, no. 1, pp. 24–33, 2005, doi: 10.2118/84228-PA.

[4] Z. Li, G. Oger, and D. Le Touzé, "A finite volume WENO scheme for immiscible inviscid two-phase flows," *Journal of Computational Physics*, vol. 418, p. 109601, Oct. 2020, doi: 10.1016/j.jcp.2020.109601.

[5] C. Berg, "Estimation of Influx and Loss During Drilling Operations Modeling for Automatic Control and Estimation of Influx and Loss During Drilling Operations A PhD dissertation in," University of South-Eastern Norway, 2020.

[6] X.-D. Liu, S. Osher, and T. Chan, "Weighted Essentially Non-oscillatory

Schemes," *Journal of Computational Physics*, vol. 115, no. 1, pp. 200–212, 1994, doi: https://doi.org/10.1006/jcph.1994.1187.

[7] C. W. Shu, "Essentially Non-Oscillatory and Weighted Essentially Non-Oscillatory Schemes for Hyperbolic Conservation Laws," *ICASE Report*, no. 97–65, 1997, doi: 10.1007/bfb0096355.

[8] S. Gottlieb and C. W. Shu, "Total variation diminishing Runge-Kutta schemes," *Mathematics of Computation of the American Mathematical Society*, vol. 67, no. 221, 1998, doi: 10.1090/s0025-5718-98-00913-2.

[9] C.-W. Shu and S. Osher, "Efficient implementation of essentially non-oscillatory shock-capturing schemes," *Journal of Computational Physics*, vol. 77, no. 2, pp. 439–471, Aug. 1988, doi: 10.1016/0021-9991(88)90177-5.

[10] A. Harten, B. Engquist, S. Osher, and S. R. Chakravarthy, "Uniformly high order accurate essentially non-oscillatory schemes, III," *Journal of Computational Physics*, vol. 71, no. 2, pp. 231–303, 1987, doi: 10.1016/0021-9991(87)90031-3.

[11] H. Nessyahu and E. Tadmor, "Non-oscillatory central differencing for hyperbolic conservation laws," *Journal of Computational Physics*, vol. 87, no. 2, pp. 408–463, Apr. 1990, doi: 10.1016/0021-9991(90)90260-8.

[12] A. Kurganov and E. Tadmor, "New High-Resolution Central Schemes for Nonlinear Conservation Laws and Convection-Diffusion Equations," *Journal of Computational Physics*, vol. 160, no. 1, pp. 241–282, May 2000, doi: 10.1006/jcph.2000.6459.

[13] E. F. Toro, *Riemann solvers and numerical methods for fluid dynamics-A Practical Introduction*, 3rd ed. Heidelberg: Springer Science & Business Media, 2009. doi: 10.1007/b7976.

[14] R. J. LeVeque, *Finite volume methods for hyperbolic problems*, 1st ed. Cambridge: Cambridge University Press, 2002.

[15] A. Kurganov, S. Noelle, G. Petrova, and S. J. C. Sci, "Semidiscrete central - upwind schemes for hyperbolic conservation laws and Hamilton – Jacobi equations," *SIAM Journal on Scientific Computing*, vol. 23, no. 3, pp. 707–740, 2001, doi: 10.1137/S1064827500373413.

[16] K. K. Fjelde and K. H. Karlsen, "High-resolution hybrid primitive-conservative upwind schemes for the drift flux model," *Computers and Fluids*, vol. 31, no. 3, pp. 335–367, Mar. 2002, doi: 10.1016/s0045-7930(01)00041-x.

[17] M. H. Abbasi *et al.*, "A Godunov-type Scheme for the Drift Flux Model with Variable Cross Section," *Journal of Petroleum Science and Engineering*, vol. 179, no. February 2019, pp. 796–813, 2019, doi: 10.1016/j.petrol.2019.04.089.

[18] C. W. Shu and S. Osher, "Efficient implementation of essentially non-oscillatory shock-capturing schemes, II," *Journal of Computational Physics*, vol. 77, no. 2, pp. 439–471, 1988, doi: 10.1016/0021-9991(88)90177-5.

[19] G. S. Jiang and C. W. Shu, "Efficient implementation of weighted ENO schemes," *Journal of Computational Physics*, vol. 126, no. 1, pp. 202–228, 1996, doi: 10.1006/jcph.1996.0130.

[20] G. S. Jiang and D. Peng, "Weighted ENO Schemes for Hamilton-Jacobi Equations," *Journal of Applied Mathematics and Stochastic Analysis*, vol. 2008, pp. 1–24, 2008, doi: 10.1155/2008/359142.